Journal of Theoretical Biology 385 (2015) 90–101

Contents lists available at ScienceDirect

Journal of Theoretical Biology

journal homepage: www.elsevier.com/locate/yjtbi

Exploring the structure and conformational landscape of human leptin. A molecular dynamics approach

Brenda Chimal-Vega [a], Norma Paniagua-Castro [b], Jonathan Carrillo Vazquez [a], Jorge L. Rosas-Trigueros [c], Absalom Zamorano-Carrillo [a], Claudia G. Benítez-Cardoza [a,*]

[a] Laboratorio de Investigación Bioquímica y Biofísica Computacional, Doctorado en Ciencias en Biotecnología, ENMH, Instituto Politécnico Nacional, Guillermo Massieu Helguera, México, D.F. 07320, México
[b] Departamento de Fisiología, Doctorado en Ciencias en Biotecnología, ENCB, Instituto Politécnico Nacional. Avenida Wilfrido Massieu s/n, Esq. Manuel L. Stampa, Col. Unidad Profesional Adolfo López Mateos, Delegación Gustavo A. Madero, 07738 México, D.F., México
[c] Laboratorio Transdisciplinario de Investigación en Sistemas Evolutivos, SEPI de la ESCOM del Instituto Politécnico Nacional, Juan de Dios Bátiz y Miguel Othón de Mendizábal s/n, México, D.F. 07738, México

ARTICLE INFO

Article history:
Received 11 March 2015
Received in revised form
21 July 2015
Accepted 17 August 2015
Available online 3 September 2015

Keywords:
Leptin
Molecular dynamics simulations
Intrinsically disordered regions
Thermal unfolding

ABSTRACT

Leptin is a hormone that regulates energy homeostasis, inflammation, hematopoiesis and immune response, among other functions (Houseknecht et al., 1998; Zhang et al., 1995; Paz-Filho et al., 2010). To obtain its crystallographic structure, it was necessary to substitute a tryptophan for a glutamic acid at position 100, thus creating a mutant leptin that has been reported to have biological activity comparable to the activity of the wild type but that crystallizes more readily. Here, we report a comparative study of the conformational space of WT and W100E leptin using molecular dynamics simulations performed at 300, 400, and 500 K. We detected differences between the interactions of the two proteins with local and distal effects, resulting in changes in the conformation, accessible surface area, compactness, electrostatic potential and dynamic behavior. Additionally, the series of unfolding events that occur when leptin is subjected to high temperature differs for the two constructs. We observed that both proteins are mostly unstructured after 20 ns of MD simulation at 500 K. However, WT leptin maintains a significant amount of secondary structure in helix α2, while the most stable region of W100E leptin is helix α3. Furthermore, we found that the region between residues 25 and 42 might adopt interconverting secondary structures ranging from α-helices and random coils to β-strand structures. Thus, this region can be considered an intrinsically disordered region. This atomistic description supports our understanding of leptin signaling and consequently might facilitate the use of leptin in treatments for the pathophysiologies in which it is implicated.

1. Introduction

Leptin is one of the most important hormones; it participates in energy homeostasis in mammals as well as in many other physiological processes, including glucose homeostasis (Paz-Filho et al., 2010; Seufert et al., 1999), fatty acid homeostasis in non-adipocytes (Unger et al., 1999), reproduction (Brenner and Makc, 2009) and sexual development (Moschos et al., 2002), immune response (Lord et al., 1998; Martí et al., 2001), angiogenesis (Sierra-Honigmann et al., 1998), wound healing (Ring et al., 2000) and bone remodeling (Ducy et al., 2000). Encoded by the *lep* or *ob* gene, leptin is mainly produced in white adipose tissue, followed by brown adipose tissue and several other tissues, including skeletal muscle, bone marrow, stomach, pituitary gland, and liver (Prins, 2002; Masuzaki et al., 1997).

The role of leptin in energy balance was noticed upon the discovery that humans and rodents lacking a functional leptin protein or receptor exhibit hyperphagia and obesity that can be solved by leptin administration (Zhang et al., 1995). However, obesity is typically associated with high leptin levels rather than leptin deficiency (Flier, 1998; Heymsfield et al., 1999).

Consequently, the use of leptin as a therapeutic option in obese patients has, in many instances, been unsatisfactory (Bence et al., 2006). Additionally, certain characteristics of leptin, such as its short circulating half-life, low potency, and poor solubility at physiological pH, have been considered limitations of leptin treatments (Lo et al., 2005). Several efforts have focused on improving leptin solubility at physiological pH (Lo et al., 2005). One of the first examples was the mutant construct W100E leptin, which shows dramatically improved solubility and a propensity to crystallize, but with comparable

* Correspondence to: Laboratorio de Investigación Bioquímica, Sección de Estudios de Posgrado, ENMyH-IPN, Guillermo Massieu Helguera No. 239, La Escalera Ticoman, D.F. 07320, Mexico. Tel.: +52 55 57296300x55562.
E-mail address: beni1972uk@gmail.com (C.G. Benítez-Cardoza).

http://dx.doi.org/10.1016/j.jtbi.2015.08.014
0022-5193/

biological activity to the activity of the wild-type protein (Zhang et al., 1997). It has been shown that the treatment of W100E leptin implanted subcutaneously in obese mice receiving high-calorie diet resulted in reduced food intake, body weight and triglycerides levels, but increased HDL-cholesterol levels (Chimal et al., 2014).

The crystal structure of leptin revealed a four-helix bundle and two relatively long interconnected loops; this structure is similar to the conformation of the long-chain helical cytokine family. Interestingly, leptin shows a unique slipknot structure created by a disulfide bridge between the C-terminus and residue 96 to make a 50-residue covalent loop. The N-terminal region threads through the covalent loop. This structure is the simplest slipknot topology described to date. Additionally, it has been demonstrated that a lack of the disulfide bridge leads to a loss of leptin functionality, resulting in morbid obesity (Boute et al., 2004). The most plausible explanation for this observation is the improper folding and knotting of the N-terminal region of leptin through the loop (Haglund et al., 2012).

Nevertheless, no thorough analysis and comparison of the conformation and dynamical properties of WT and W100E human leptin have been performed since the report of the crystal structure of W100E leptin.

"Since the pioneer paper entitled 'The Biological Functions of Low-Frequency Phonons' (Chen et al., 1977) was published in 1977, a series of investigations into biomacromolecules from dynamic point of view have been stimulated. These studies have suggested that low-frequency (or terahertz frequency) collective motions do exist in proteins and DNA (Forsen et al., 1981; Chou, 1985; Maggiora et al., 1989; Martel, 1992; Zhou, 1989; Bax et al., 2001; Sinkala, 2006). Furthermore, many important biological functions in proteins and DNA and their dynamic mechanisms, such as switch between active and inactive states (Wang et al., 2009a, 2009b, 2009c), cooperative effects (Chou, 1989), intercalation of drugs into DNA (Mao et al., 1988), and assembly of microtubules (Maggiora et al., 1994), can be revealed by studying the low-frequency internal motions as summarized in a comprehensive review (Chou, 1998). Some scientists even applied this kind of low-frequency internal motion for medical treatments (Gordon, 2007', 2008; Madkan et al., 2009). Actually, investigation into the internal motion in biomacromolecules and its biological functions is deemed as a "genuinely new frontier in biological physics", as announced by the Vermont Photonics in an article at http://www.vermontphotonics.com/NewFrontierBiophysics.pdf. In view of this, to really understand the action mechanisms of biomacromolecules, we should consider not only the static structural information but also the dynamical information acquired by studying their internal motions. Molecular dynamics (MD) simulations are a powerful theoretical approach that can successfully complement and extend the experimental results and reproduce them with reasonable accuracy (Daggett, 2006; Day et al., 2010). Recently, MD simulations have been used to study the switch mechanism of human Rab5a (Wang, 2009), the inhibition mechanism of PTP1B (Wang et al., 2009a, 2009b, 2009c), the gating and inhibition mechanism of the M2 proton channel from influenza A viruses (Wang and Wei, 2009) based on the NMR structure (Schnell and Chou, 2008; Pielak et al., 2009), the personalized drug design (Wang et al., 2008a, 2008b, 2007a, 2007b), the enzyme-ligand binding interaction (Wang et al., 2008a, 2008b, 2007a, 2007b), the binding mechanism of H5N1 influenza virus neuraminidase with ligands (Gong et al., 2009), the metabolic mechanism (Wang et al., 2009a, 2009b, 2009c), and the binding mechanism of calmodulin with chrysin (Li et al., 2007).

In this work, we obtained the full-length protein structures of the WT and W100E leptin constructs using the widely used protein-structure predictor I-TASSER, which combines threading alignments with *ab initio* procedures. Additionally, we used molecular dynamics (MD) simulations at different temperatures to thoroughly analyze and compare, for the first time, the conformational spaces of wild-type human leptin and its soluble mutant W100E. Differences in the secondary structure propensities, electrostatic and hydrophobic interactions, dynamical properties and conformational stability of the constructs could be identified. The structure and dynamical properties of the obese hormone protein must be described on an atomistic basis to shed light on its biological activity and physicochemical properties. This information will be useful in overcoming the inherent limitations that impede the use of leptin in treatments for obesity and other pathophysiological disorders in which leptin is implicated.

2. Materials and methods

2.1. Theoretical procedure-three-dimensional structure of WT and W100E leptin models

To obtain the initial coordinates of WT and W100E human leptin, we constructed 3D models using the I-TASSER server (Zhang, 2008). The crystallographic structure of W100E leptin that is reported in the protein data bank with the PDB ID 1AX8 was used as a template (Zhang et al., 1997). I-TASSER predicted the full-length leptin structure by combining threading and *ab initio* modeling. The sequence of each construct was submitted independently to the I-TASSER server, which provided five modes for each protein. For the sake of comparison, we also used the programs Modeler (⟨https://salilab.org/modeller/⟩; Eswar et al., 2006; Webb and Sali, 2014) and MOE (Molecular Operating Environmet versión 2008.10.) for structure prediction. The best model was selected after an analysis of the structures using Ramachandran plots (Laskowski et al., 1993, 1996), root mean square deviation (RMSD), and the programs VERIFY3D (Lüthy et al., 1992), PROCHECK (Laskowski et al., 1993, 1996) and Solvx (Holm and Sander, 1992). The best models were used to provide the initial coordinates for the remaining the MD simulations. The electrostatic potential at the surface of the molecules was calculated by solving the Poisson Boltzmann equation using a plugin for the PyMOL molecular graphics program (⟨http://www.pymol.org⟩).

2.2. Normal mode analysis

The normal low-frequency vibrational modes of both leptin constructs were analyzed using the elastic network model, which is implemented with the "rotation-translation-block" approximation in the web interface ElNemo. This analysis identifies potential conformational changes in proteins (Suhre and Sanejouand, 2004; ⟨http://igs-server.cnrs.mrs.fr/elnemo/index.html⟩; Tama et al., 2000; Delarue and Sanejouand, 2002). The following key parameters were used: DQMIN = −100, DQMAX = 100, DQSTEP = 20 and NRBL = auto. We analyzed the structural characteristics, the collectivity of the atomic movements of a total of 106 residues and the low-frequency normal modes.

2.3. Molecular dynamics simulations

MD simulations were performed using GROMACS 4 (Hess et al., 2008) with the OPLS-AA force field (Jorgensen and Tirado-Rives, 1998). The leapfrog algorithm for integrating Newton's equations was used, and periodic boundary conditions were applied. The protein was solvated in a rectangular box of SPC water (Berendsen et al., 1981) with a minimum distance of 1 nm from the protein to the edge of the box. To obtain a neutral total charge in the system, four Na^+ counterions were added for W100E and three for WT. The total sizes of the systems were 23,073 and 23,160 atoms, including 6933 and 6536 water molecules, for W100E and WT, respectively. All bonds were constrained using LINCS (Hess et al., 1997). During energy minimization, the steepest descent algorithm was used, and convergence was reached in 200 steps. Further equilibration of the system was

accomplished in 5000 steps (10 ps) of MD simulation with restricted protein atoms and NVT conditions with a box size of 5.73, 6.003 and 6.868 nm for W100E and 5.72, 5.785 and 6.963 nm for WT. Afterwards, both systems were subjected to the same protocol. The protocol began with 20 ns of MD at 300 K without any atom fixing; that outcome was used as a starting point for 20 ns of MD at 400 K, and the subsequent outcome was used as a starting point for 20 ns of MD at 500 K. MD simulations were performed with a time step of 2 fs under NPT conditions such that the size of the box could fluctuate to keep the pressure at a constant value, and the coordinates for the whole system were saved every 250 steps. For all MD simulations, neighbor lists were updated every 10 steps. The PME algorithm (Essmann et al., 1995) was used for the electrostatic interactions with a cutoff of 1 nm, and a reciprocal grid of 0.12 cells was used with 4th order B-spline interpolation. A single cut-off of 1 nm was used to calculate the van der Waals interactions. Temperature and pressure coupling were performed with the Nosé–Hoover algorithm (Nosé and Klein, 1983; Parinello and Rahmand, 1981) and the Parrinello–Rahman algorithm, (Nosé, 1984; Hoover, 1985), respectively. After stabilization of the system, the potential energy was conserved in all cases during the MD simulations. The analysis tools included in GROMACS were used to calculate the RMSD, RMSF, Rg, and SASA. The evolution of the secondary structure was followed using the DSSP program (Kabsch and Sander, 1983). Graphical representations of the models were obtained using VMD 1.9.1 (Humphrey et al., 1996). All MD simulations were performed by triplicate.

2.4. Disordered tendency prediction

Intrinsically unstructured/disordered regions within both constructs of leptin were predicted using the IUPred algorithm, which assumes that folding, is unlikely in these intrinsically disordered regions or proteins due to their inability to form sufficient stabilizing inter-residue interactions (Dosztányi et al., 2005). The parameter set best suited for predicting short disordered regions was employed.

3. Results

We were not able to find any reports using precisely this construct in similar studies. Commonly Leptin treatments are carried out using either metreleptin or a variety of mutants or analog constructs with different composition to W100E Leptin. Considering that a single point mutation might be sufficient to modify the conformation, stability and functionality of any protein; we were motivated to make a detailed study on the conformational and molecular dynamics of WT and W100E leptin.

3.1. Three-dimensional structure of WT and W100E leptin constructs

The crystallographic structure of W100E leptin was obtained almost two decades ago (PDB ID 1AX8). This structure lacks residues (Houseknecht et al., 1998; Zhang et al., 1995) 25–38. We obtained the full-length WT and W100E leptin structures using several modeling programs. Ramachandran plots, RMSD values, and structural analysis of the models indicated that the I-TASSER server provided the best structures (**Table 1**), which are shown in Fig. 1. As expected, the characteristic large, hydrophobic and cylindrical core of the leptin structure is highly conserved. *Ab initio* procedures predicted different secondary structures for residues 25-38 of the two molecules. For the WT human leptin, this region was modeled as a loop, while the W100E mutant showed the formation of an α-helix involving residues 34–41. To confirm this observation, we performed a thorough inspection of this region for all models provided by the I-TASSER server, as well as for the models produced by other structure predictors, such as MOE and Modeler. The resulting models all indicated

Table 1
Comparison of model performance in terms of structural analysis

Model	PROCHEK (Laskowski et al., 1998, 1996)Residues in most favored regions	SOLVX (Holm and Sander, 1992)	ANOLEA (Melo et al., 1997) Total number of non-local atomic interactions	VERIFY3D (Lüthy et al., 1992)
1AX8	94.7%	0	11,048	0.30
I-Tasser	92.3 %	0	11,860	0.30
Modeler	81.5%	0	12,576	0.30
Moe	0%	0	13,158	0.35

that residues 34 to 41 are prone to a helical conformation in W100E leptin, while the same amino acid residues in WT leptin do not show this propensity.

Furthermore, we calculated the electrostatic potential of the surfaces of WT and W100E leptin (Fig. 1B and C). There is a large positive area in WT leptin near position 100, whereas this area is modified to be more negative in the W100E mutant.

The conformational landscape of WT and W100E leptin was explored by MD simulations at 300, 400 and 500 K for 20 ns. Some structural parameters were examined and are shown in Fig. 2. In the following results, we note the similarities and differences between the trajectories of WT and W100E leptin.

3.2. Root mean square deviation (RMSDα) values

The root mean square deviation of the α-carbons (RMSDα) of the models allows a comparison of the global movements of the models, as shown in Fig. 2A and B. Initially, the RMSDα values increase in the MD simulations during the equilibration period upon heating of the system. On average, for both proteins, the RMSDα values were approximately bounded between 0.2 and 0.4 nm at the temperatures of 300 K and 400 K, although certain differences occurred in the profiles of the curves for each protein. We observe that at 300 K, WT leptin shows a long plateau at approximately 0.22 nm, with an abrupt increase of the RMSD value to approximately 0.38 nm at approximately 9.5 ns. This abrupt change is coincident with changes in the helical content of two helices; helix α3 is partially lost, while helix α2 becomes more structured. At that time, we also observe a reduction of SASA. Meanwhile, for the mutant protein at 300 K, we do not observe any rapid increments of the RMSDα values; instead, the values gradually increase during the MD simulation. At 400 K, the WT construct shows an RMSDα value of approximately 0.24 nm for the first 1.2 ns of the simulation. At approximately this time, the RMSDα value increased to approximately 0.4 nm and remained at that value until the end of the trajectory. For W100E leptin at 400 K, we observe similar RMSDα values bounded between 0.2 and 0.4 nm. In this case, the RMSDα values ranged from approximately 0.2 to 0.25 nm for 9.5 ns of the simulation, after which we detected an increment in the RMSDα value to approximately 0.4 nm for the rest of the simulation. At 500 K, for both proteins, we observe important increments in the RMSDα values from 0.4 to 1.4 nm. For the WT protein, equilibrium is reached at approximately 5 ns. In contrast, the mutant shows a long plateau for the first 5 ns of the experiment; this plateau occurs from 0.7 to 0.8 nm, and the RMSD slowly increases starting at approximately 8.5 ns to reach an RMSD value of approximately 1.2–1.3 *circa* 17.5 ns. On average, the WT leptin stabilizes more quickly than the mutant at the three tested temperatures; this finding indicates that apart from differences in the secondary structure, the W100E leptin mutation also promotes continuous movement during the molecular dynamic simulation. To group the conformations according to the RMSD value, we performed clustering analysis (Fig. 1S). We were able to recognize at least two main patterns in each construct at every studied temperature. Specifically, WT human leptin shows three

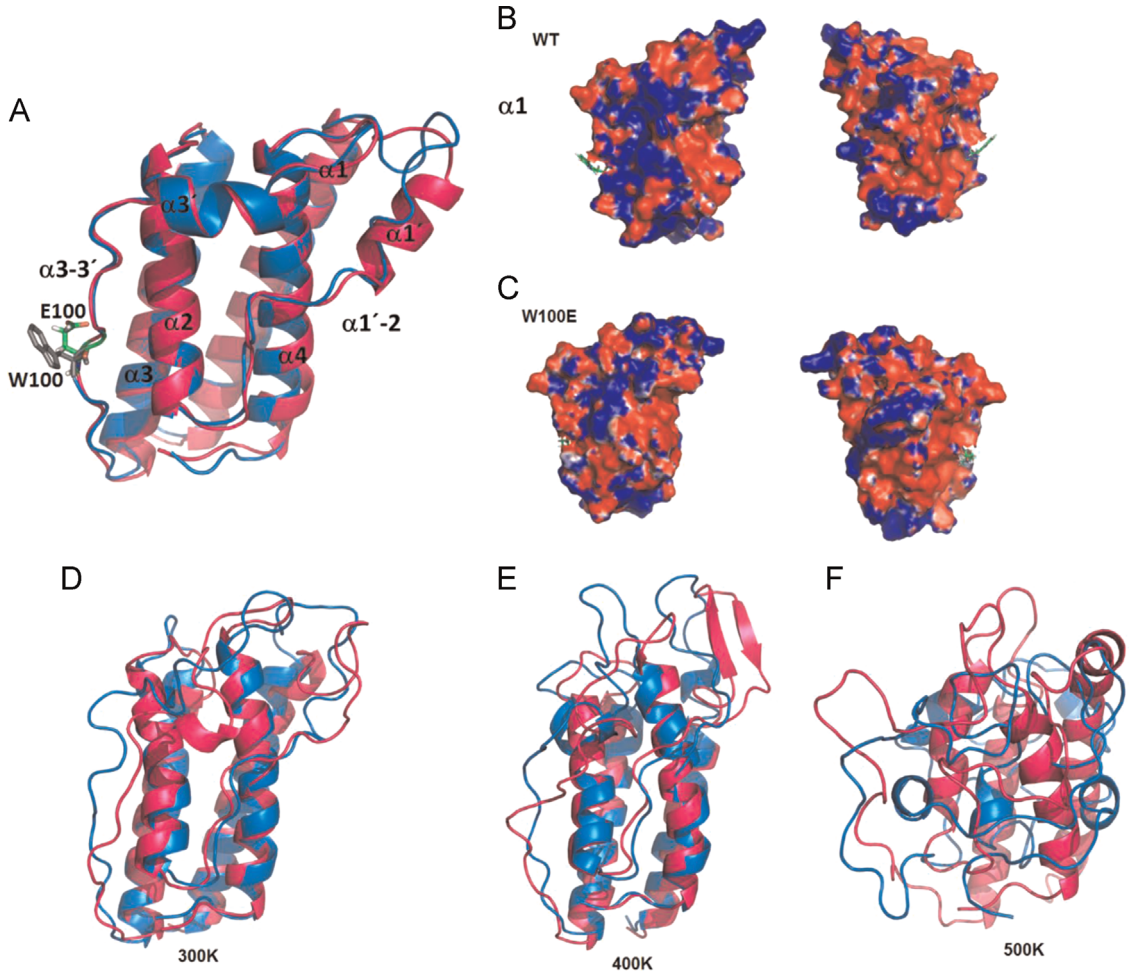

Fig. 1. Structural model of Leptin. The helices α1, α1', α1'-2, α2, α3, α3', α3-3' and α4 are indicated. (A) Superimposed structure of WT (blue) and W100E (pink) Leptins. The mutation at position 100 is indicated tryptophan (gray) and glutamic acid (green). (B) Surface electrostatic potential of WT Leptin, and (C) surface electrostatic potential of W100E Leptin. (D, F, G) Average structures of WT and W100E Leptins at 300 K, 400 K, and 500 K. The Connolly surfaces of the proteins were created using the PyMol program [http://www.pymol.org] The electrostatic potential is indicated by the color saturation (red for negative and blue for positive). (For interpretation of the references to color in this figure legend, the reader is referred to the web version of this article.)

groups of conformations at 300 K and at 500 K, whereas it shows 2 main ensembles of conformations at 400 K. W100E leptin can be represented by two, three and four main clusters at 300, 400 and 500 K, respectively.

3.3. Radius of gyration (RG)

The fluctuating RG values demonstrate the conformational movements of the whole protein. The radius of gyration (RG) values of WT and W100E leptin are shown in Fig. 2C and D. At 300 and 400 K, the starting value for both proteins is approximately 1.55 nm. This result confirms that mutation does not substantially alter the compactness of leptin. During the MD simulations at 300 and 400 K, the RG value fluctuates between 1.55 and 1.62 nm, whereas the RG values at 500 K for both proteins show larger fluctuations from 1.6 to 1.72 nm. For the WT protein in particular, the starting value is approximately 1.65 nm, and the endpoint is 1.45 nm, indicating a small reduction in the overall elongation of the molecule. Interestingly, this construct shows RG values below 1.55 for long periods during the second half of the simulation. In contrast, W100E leptin shows RG values below 1.55 for shorter periods in conjunction with periods with RG values *circa* 1.65, indicating alternating events of expansion and contraction of the molecule. On average, at 500 K, W100E seems to be less compact than the WT protein.

3.4. Solvent-accessible surface area (SASA)

The solvent-accessible surface area (SASA) profiles of WT and W100E leptin throughout the simulations are shown in Fig. 2E and F, respectively. Panel E shows that the SASA values for the WT protein are bounded between 85 and 97 nm^2 at 300 K throughout the simulation, with the smallest values between 10 and 15 ns. At 400 K, the values oscillate between 86 and 93 nm^2. At 500 K, the values increased and then oscillated at approximately 95 nm^2. In contrast, the mutant leptin at 300 K also shows SASA values bounded between 85 and 97 nm^2 but with higher frequency oscillations than WT; however, at 400 K, the values oscillate from 83 to 95 nm^2, with the largest values during the last two nanoseconds of the simulation. At 500 K, W100E leptin shows an important increase in SASA; on average, the SASA values oscillate at approximately 110 nm, with some points reaching values greater than 115 and 120 nm^2.

3.5. Root mean square fluctuation (RMSF) values

To explore the global backbone deviation, the RMSF values are presented in Fig. 2G and H. At 300 and 400 K, we observe smaller values for the structured regions than for the loops. The unstructured regions occur in roughly the same residue ranges in the mutant leptin as in the wild type. The RMSF values for both proteins within the structured regions are close to 0.1 nm and 0.2 nm at 300 and 400 K,

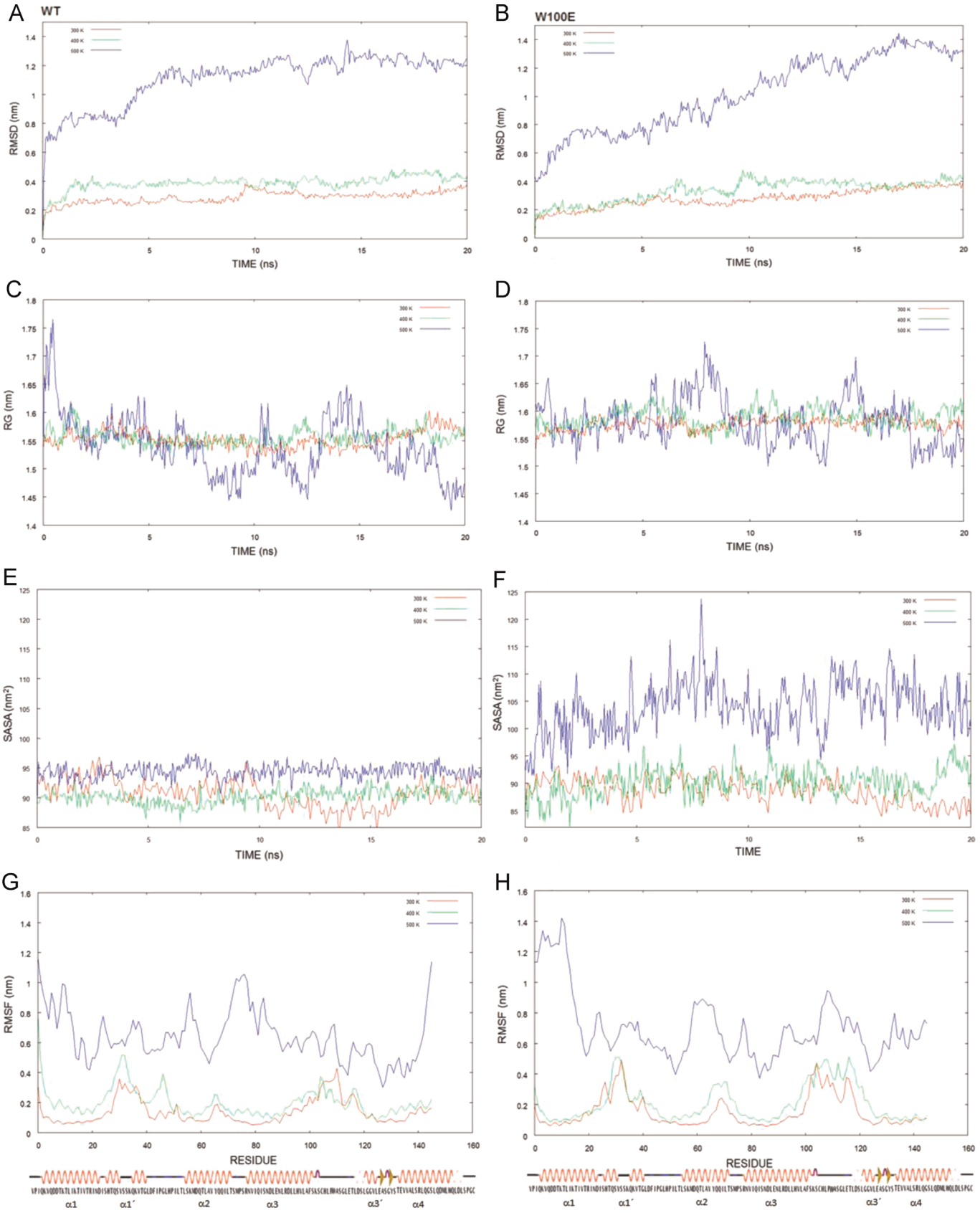

Fig. 2. Structural analysis from the MD simulations of WT (A, C, E, G) and W100E (B, D, F, H) human leptin. Time evolution of (A, B) α-carbon RMSD, (C, D) radius of gyration, and (E, F) solvent accessible surface area of the protein at three different temperatures. (G, H) The root mean square fluctuations of the α-carbon coordinates are shown as a function of residue number; at the bottom, a representation of the secondary structure with labels for the main domains is included. The colors indicate the temperature of the MD simulation: 300 (red), 400 (green) and 500 K (blue). (For interpretation of the references to color in this figure legend, the reader is referred to the web version of this article.)

respectively. However, there are certain changes in these profiles for each protein. In particular, at 300 K, the observed differences include the following: the WT leptin shows RMSF values centered at 0.35 nm in the region from residues 25 to 39. In contrast, this mobile zone includes residues 23 to 41 in W100E leptin; on average, the values are slightly higher, with some RMSF values of 0.4 nm. Certain distinctive interactions might be responsible for the lower mobility (higher rigidity) of residues 28–40 in the WT leptin. Another flexible region involves residues 100–118. The RMSF values for the residues in this region are higher for W100E leptin than for the WT protein. Regarding the MD smulation at 400 K, residues 43–50 in the WT protein show an increment in the RMSF values that is not observed in the mutant protein. Furthermore, in the mutant protein, we observe increased mobility in the regions between residues 65–95 and 100–120. At 500 K, the RMSF values of both proteins are mostly above 0.4 nm. For W100E leptin, we observed the largest RMSF values for residues 1–17; the rest of the protein shows a global deviation that fluctuates between 0.5 and 0.9 nm. In contrast, at this temperature, the RMSF values of WT leptin fluctuate between 0.5 and 1 nm. In particular, the mutant protein shows larger RMSF values in the N-terminus (residues 1–17) and in the regions including residues 60–70 and 105–120. Meanwhile, WT leptin has the largest fluctuations in the N- and C-termini and in residues 75–82. It is important to note that this region corresponds to helix 3. This helix and helix 1 are the main contributors to the interaction with all isoforms of the leptin receptor.

On average, W100E leptin is more exposed to the solvent (higher SASA values), is more expanded (higher Rg values) and takes a longer time to reach equilibrium during the simulation.

3.6. Secondary structure

The time course evolution of the secondary structure of the WT and W100E leptin constructs at three different temperatures is shown in Fig. 3. At 300 K, both proteins mostly retain their secondary structures. In the WT protein (Fig. 3A), helix α1 (residues 3–25) is maintained throughout the simulation, whereas the C-end of the

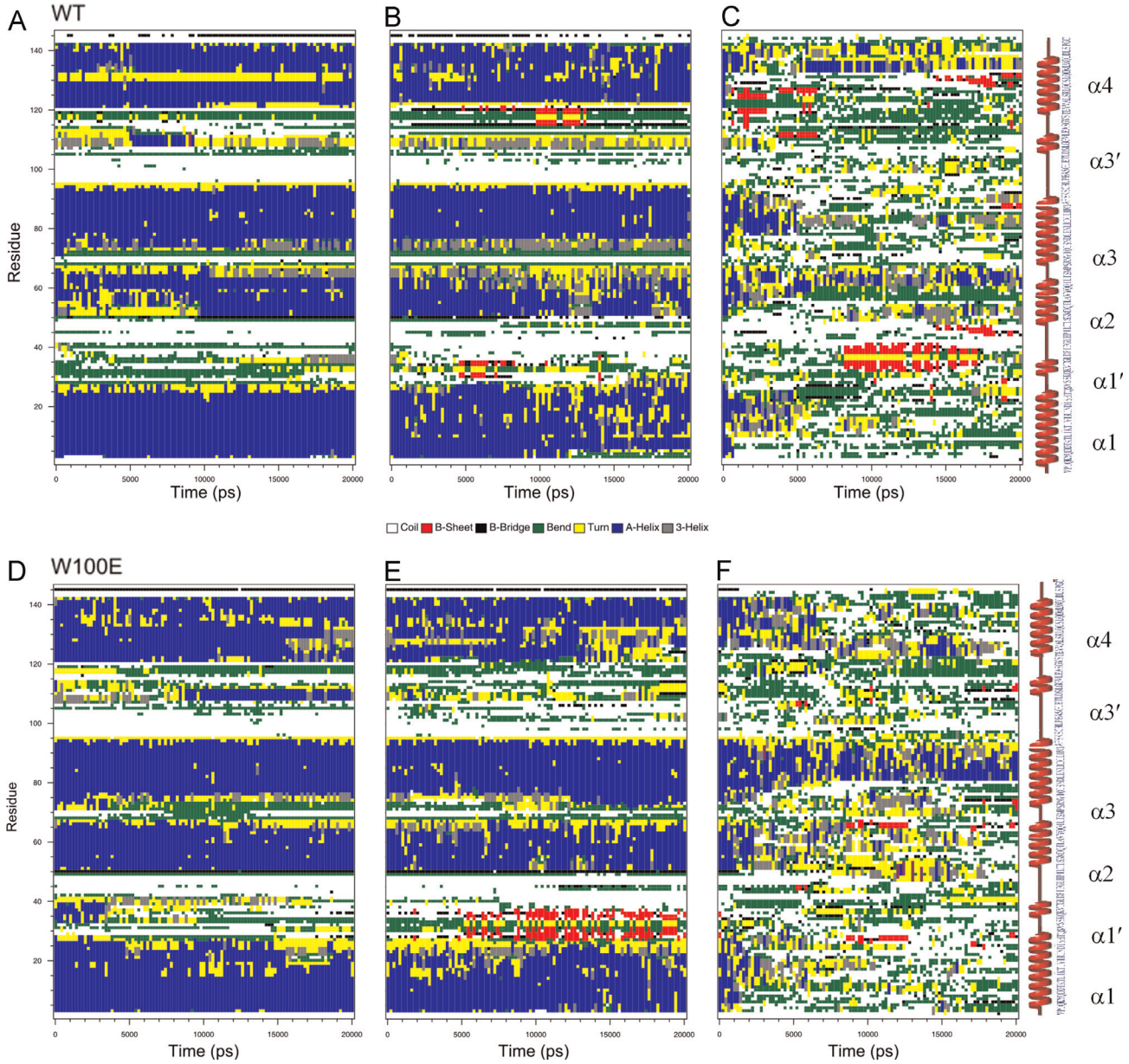

Fig. 3. Time course evolution of the secondary structural elements of WT (A–C) and W100E (D–F) leptin during simulations. (A and D) 300, (B and E) 400 and (C and F) 500 K. The colors are according to the DSSP classification. (For interpretation of the references to color in this figure legend, the reader is referred to the web version of this article.)

same helix in W100E (Fig. 3D) shows a tendency to adopt a turn conformation for approximately one-third of the simulation period. In contrast, helix α2 in the mutant protein appears to be more stable during the simulation at 300 K than in the WT leptin. Helix α3 is the most stable region in both proteins, while helix α4 seems to lose its helical content surrounding residue 130 during most of the simulation in WT leptin. In contrast, helix α4 of W100E leptin seems to be more stable during the MD simulation. The residues surrounding position 110 show a tendency to adopt a helical conformation in both proteins. This susceptibility is more persistent in W100E leptin. At 400 K (Fig. 3B and E), both proteins show higher fluctuations in their helices. Residues 28–38 show a propensity to adopt a β-sheet conformation. Although this tendency also occurs in the WT protein (roughly 20% of the MD simulation), it is much more persistent in the mutant protein (approximately 70% of the time span of the MD simulation). Residues 110–120 of the WT protein also show this propensity, which is noticeably greater in the WT protein. At 500 K, both proteins show an important loss of secondary structure (Fig. 3C and F). In WT leptin, helices α1 and α3 are fully unstructured before 5 ns, while helices α2 and α4 show certain fluctuations between helical and turn conformations; however, the helical conformation predominates in helix α2, and the turn conformation predominates in helix α4. The residues from 34 to 41 show a propensity to adopt a β-sheet conformation for approximately 50% of the duration of the simulation at 500 K. Helix α3 in W100E leptin shows helical content throughout most of the simulation, while the rest of the protein does not conserve its secondary structure. The tendency to adopt a β-strand structure is much lower in the mutant protein and is only partially observable in helix α1′and at the end of α2.

3.7. Native state of WT and W100E leptin

WT and W100E leptin show different profiles in their molecular dynamics. InFig. 4, we show certain representative images illustrating this statement. At 300 K, the overall conformation of helices α1, α2, α3 and α4 does not substantially change in WT leptin. Some of the most appreciable movements are the extension of α3' to form a loop that approaches the loop between α3–α3′ (residues 100–120) and helix α4, causing a bending of this helix. Additionally, α1′ oscillates between helix and loop conformations during the simulation. At 400 K, helices α3 and α4 are mostly conserved during the simulation. In contrast, helices α1′ and α3′ are mainly unstructured, while the C-terminal half of helix 2 loses helicity and forms a loop, and helix α1 oscillates between unstructured and helical conformations.

Regarding the structural changes of the mutant protein, we observe that at 300 K, helices α1′ and α3′ lose their helicity (Fig. 4A1-ii,-iii), while α1, α2, α3 and α4 are conserved and remain almost intact throughout the simulation. At 400 K, the helix α1′ shows a tendency to adopt a β-strand structure, while α3′ seems to be unstructured and approaches helix α4. The loop between α3 and α3′ rotates and approaches the core of the protein. At this temperature, α1, α2, α3 and α4 are mostly intact. Additionally, as mentioned above, the coordinates of α1′ were built using *ab initio* procedures in the I-TASSER modeler; α1′ was modeled as a helical region in W100E, while it was presented as an unstructured region in the WT protein. MD simulations showed that the helical content of residues 25 to 38 does not remain throughout the simulation of the mutant protein.

The average structure obtained from clustering analysis (Fig. 1D) for the WT and W100E human leptin constructs at 300 K are almost superimposable; the only detected differences detected are the formation of a small helix (α3′) in the region between residues 106 and 115 in the W100E leptin while this region is fully unstructured in the WT leptin. In addition, the position of the loops changes with respect to the main core of the protein. At 400 K, the more relevant differences in the average structures of WT and W100E leptin are the appearance of two beta-strands formed by residues 26–41 in the mutant protein but not in the WT leptin (Fig. 1E).

By analyzing the average structures from the clustering analysis in the two constructs (Fig. 1F), we conclude that on average, W100E leptin seems to be more resistant to thermal treatment and shows important conservation of the four core helices of its structure while the WT leptin seems to be more unstructured on average. Thus, on average, W100E leptin might be described as a more stable construct than WT leptin.

3.8. Unfolding reaction of WT and W100E leptin

At 500 K, both proteins lose most of their secondary structure [Fig. 4A(3)], but the series of events that form the unfolding pathway are different in each construct. In the WT protein, α1 is the first helix to lose its helical conformation; the loop between α3 and α3′ moves away from the main core of the protein. Afterwards, helix α4 is highly unstructured and tends to lose its helicity, but during the course of simulation, it is able to recover part of its native-like secondary structure. Helix α3 is conserved for approximately 5 ns of the simulation, but after this time, it also loses its helicity. The protein is largely unfolded by 10 ns of simulation. However, the WT leptin maintains, at least partially, the helical content of helix α2. We determined that the interactions between Ile64-Leu90-S67 and Thr27-Leu126 have an important effect that maintains the integrity of helix α2.

In the mutant protein, helix α1 is the first to lose helicity, followed by α3′, which is later transformed into a loop that combines with the loop between α3 and α3′. In conjunction, this long loop appears to have very high mobility and extends away from the core of the protein. This extension causes a deformation of helix α2, and afterwards, α4 starts to lose its helical content. Later, α2 becomes fully unstructured, followed by helix α4. In this case, neither α2 nor α4 are able to recover their helical content upon denaturation. Interestingly, helix α3 is mostly conserved throughout the course of the 20 ns of simulation at 500 K. As has been mentioned, helix α3 is an important participant in the interaction of leptin with all isoforms of the leptin receptor. It is remarkable that a single point mutation is able to modify the dynamics and temperature stability of this region of the hormone protein. This helix is contiguous with the loop that harbors residue 100. We thoroughly explored the differences in the interactions between the WT and W100E leptin constructs near the mutation region. We discovered that the network of hydrogen bonding is not substantially modified between the constructs (data not shown). We identified a distinctive interaction in the mutant protein that is absent in the WT leptin: the network of electrostatic interactions between Q56, R84 and E100 (Fig. 5D). We noticed that these residues are positioned in a triangular shape, and therefore, the perimeter of this triangle is proportional to the distances between each pair of the three amino acid residues. To evaluate the persistence of this interaction network, we calculated the evolution of the triangle perimeter in both constructs during the time course of simulations (at 300 K and 500 K; Fig. 5E). The perimeter of this triangle is consistently shorter in the mutant protein than in the WT construct. This result indicates that the distances among Q56, R84 and E100 are constantly smaller than the distances among Q56, R84 and W100. Therefore, we postulate that this interaction network might be responsible for maintaining the helical content of helix α3 of W100E leptin.

3.9. Normal mode analysis

Normal mode analysis of the native structures of both leptin proteins was also performed to identify potential conformational

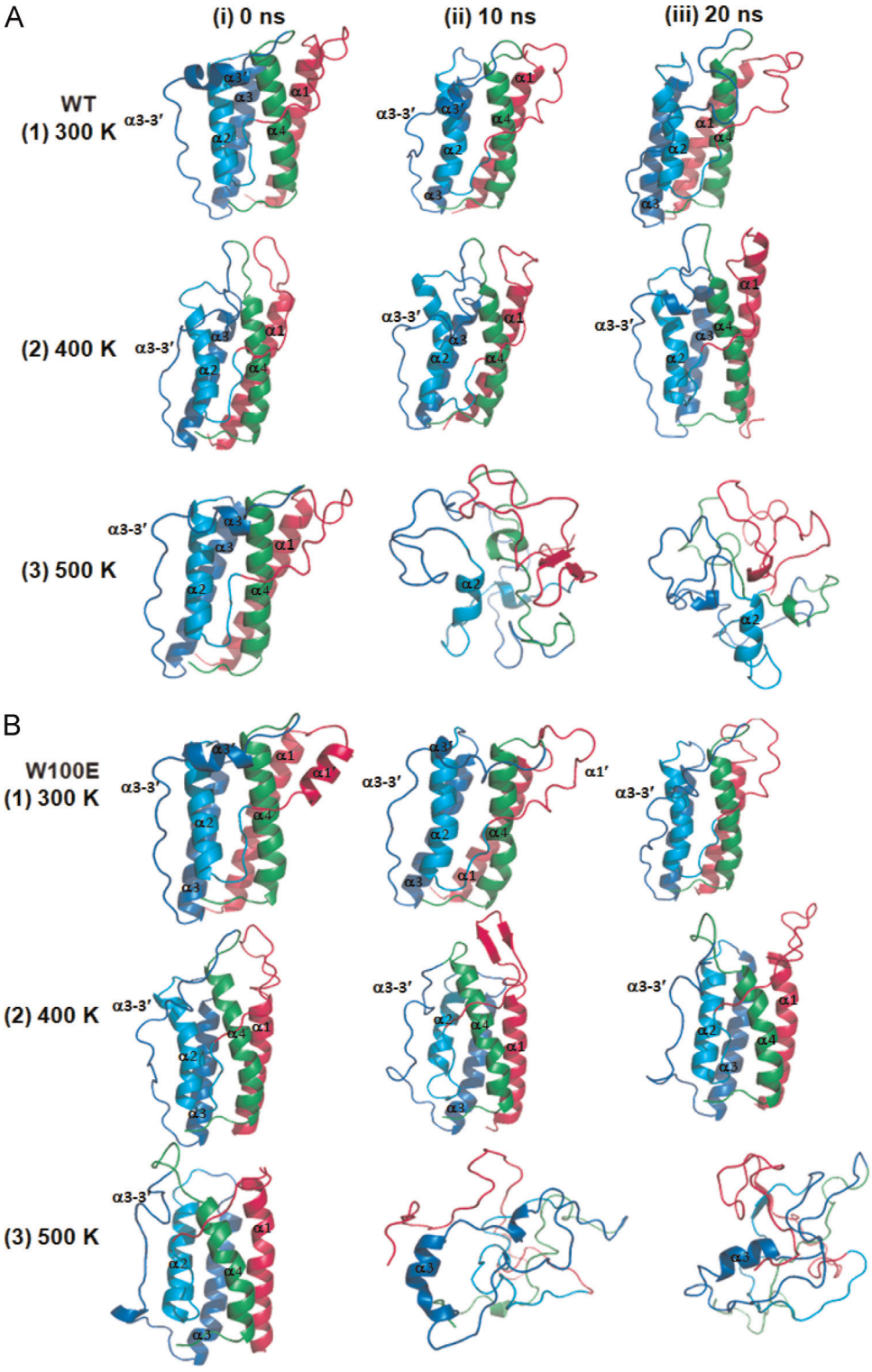

Fig. 4. Representative snapshots of the trajectory followed by WT (A) and W100E (B) leptin. The temperatures and times of simulation are indicated. The protein coloring indicates (pink) residues 1–44 helix α1–α1', (cyan) residues 45–69 helix α2, (blue) residues 70–116 helix α3 and (green) residues 117–146 helix α4. (For interpretation of the references to color in this figure legend, the reader is referred to the web version of this article.)

changes of the proteins (data not shown). Of particular interest are modes from 7 to 11; in both proteins, the frequency of these modes is low and there are large collective motifs is high. The region from residues 26 to 41 has the highest mobility in both constructs, and the mobility is slightly larger for the WT. Another zone with high mobility is the region between residues 95 and 120. In both cases, this finding is consistent with the RMSF results. Another flexible zone identified by the ElNemo server was residues 48–53; this region is located in the loop between α1′ and α2. The mobility of this last region is not appreciable in the RMSF plots. The N-terminal region seems to be more flexible in the W100E mutant than in the WT leptin.

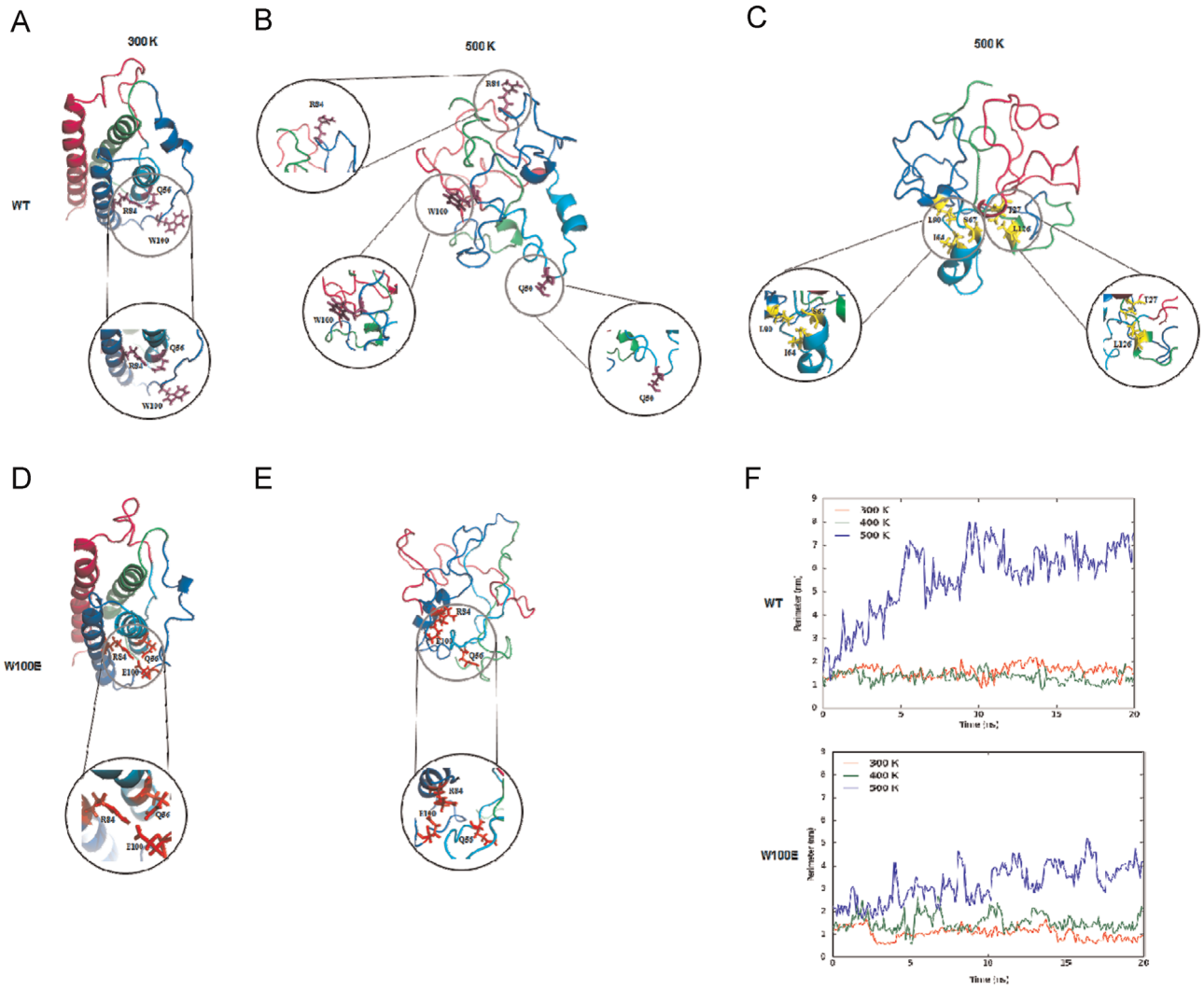

Fig. 5. Interactions between Arg 84, Gln 56 and W/E at position 100 of human leptin. (A) WT leptin at 300 K, (B and C) WT leptin at 500 K, (D) W100E leptin at 300 K, and (E) W100E leptin at 500 K. The coloring of the residues is the same as in Fig. 4. (F) Time course evolution of the perimeter of the triangle formed between R84, Q56 and W/E at position 100 of human leptin measured at 300 and 500 K.

4. Discussion

Leptin is implicated in a variety of physiological processes. The best-described process is its participation in energy homeostasis. Several efforts have been made to use this protein and its mutants to treat obesity and other related pathologies, such as lipodystrophy and diabetes. Nevertheless, the impact of mutations on the molecular dynamics and stability of leptin has not been fully assessed. In addition, the reports of the structure and molecular dynamics of leptin refer solely to the mutant in the crystallographic studies, W100E. However, to our knowledge, the structure and dynamical properties of the mutant have not been compared to those of the WT protein. Here, we have explored for the first time the conformational space of human leptin and its soluble mutant W100E leptin at different temperatures. We observed that this single point mutation is sufficient to alter the structure and conformational movements of human leptin.

First, we obtained the coordinates of the full-length WT and W100E leptin constructs. This first step was necessary because the crystallographic structure of human leptin is missing residues 25–38. I-TASSER and certain other modelers modeled this region differently in the WT leptin than in W100E leptin. The region was modeled as an unstructured region in WT leptin, but for the W100E mutant, this region was predicted to be a helix (residues 34–41). In addition in a future research it might be interesting to further explore this region using, the molecular force called polar hydrogen–π interaction (Hp–π), which may play an important role in supporting the backbones of protein loops (Du et al., 2014). During the simulations, the two proteins showed different behavior at the temperatures tested. This result demonstrated that the substitution of a single amino acid residue led to differences in the conformational movements of human leptin. These differences occurred near the mutation as well as at distal sites. Additionally, the electrostatic potential of the surface of the protein differs in the two constructs. These conformational and dynamical behavior changes might lead to the increased propensity of W100E to crystallize without effects on its biological activity because the mutation does not reside in the main regions that have been reported to be involved in the interaction of leptin with its receptor.

4.1. Amino acid residues 25–41 are defined as a putative intrinsically disordered region

Residues 25–38 show poor electron density in the crystallographic analysis (Zhang et al., 1997). Certain studies have investigated the molecular dynamics of W100E human leptin. One example is a report from Onuchic´s group, who constructed a Cα-model and performed all-atom simulations of W100E leptin; the investigation focused on

the role of the disulfide bridge formation on the local and distal motions of the peptide hormone (Carpenter et al., 2012). More recently, W100E leptin in complex with its receptor was modeled to perform a high-throughput virtual screening to design new agonizts for leptin (Fernandez Fuentes et al., 2006). In the first case, ArchPRED (a template based loop structure prediction server) (Tutone et al., 2014) was used to model the region from amino acid residues 25 to 38. The second study used the I-TASSER modeler to obtain the full coordinates of this region, similarly to our method. We obtained models that indicated that the secondary structure of this region differed between WT and W100E leptin. Furthermore, during the simulations at 300 and 400 K, this region in conjunction with residues 25–41 showed a tendency to adopt either a turn conformation or a β-strand structure. These intriguing results led us to postulate that residues 25–41 constitute a putative intrinsically disordered region (IDR). Therefore, we performed a thorough analysis to confirm this hypothesis. We used the IUPred program (Dosztányi et al., 2005) to further investigate the tendency for the region containing residues 25–41 in human leptin to become disordered. We observed that this region shows the highest tendency to become disordered within the whole length of both proteins (Fig. 2S), even higher than the N- and C-termini. Furthermore, normal mode analysis using the ElNemo server indicated that this region has the highest mobility within the whole structure in both leptin constructs. Intrinsically unstructured regions in proteins have no single well-defined tertiary structure in their native state. Similar to other intrinsically disordered regions or proteins, the 25–41 region resembles the denatured state of a protein and seems to interconvert among alternative structures; the region also has some tendency to form local secondary structure elements, either an α-helix or β-strand structure. This finding raises a crucial question: why does leptin need an IDR? One possibility might be to facilitate the interaction of leptin with its receptor. To date, helices α1 and α3 have been described as the main regions responsible for this interaction. IDRs have been identified as having important roles in molecular recognition, for which structural disorder confers specific advantages, such as increased speed of interaction and specificity without excessive binding strength. Disordered regions can also constitute flexible linkers or spacers with a role in forming macromolecular assemblies, which raises the possibility that the region between residues 25 and 41 might also be involved in the cell signaling of leptin. Another plausible reason for the presence of an IDR within the leptin structure might be to facilitate the threading of the N-terminus through the covalent loop (residues 96–146) to form the characteristic slipknot of the leptin structure. Further investigation is required to confirm either of these two possibilities or to propose another possible explanation.

4.2. *Unfolding pathway of the slipknotted human leptin*

The unique topological feature of leptin is the formation of a slipknot in which the N-terminal region threads across a covalent loop formed by a disulfide bridge between the C-terminus and residue 96; this feature makes exploring the conformational space and unfolding pathway of leptin interesting and challenging. Here, we subjected the coordinates of WT and W100E leptin to molecular dynamics simulations at 500 K. Both leptin constructs lost their native structure during the simulations at this temperature, but we observed different unfolding pathways for the two leptin constructs. In both cases, we observed that the most unstable region corresponds to α1. Another conformational change observed during the unfolding of leptin was that the loop between α3 and α3´ became more mobile and separated from the main core of the protein. Next, helical content of α2 and α4 was lost, but in the WT protein, these two helices (mainly α2) are prone to recovering part of their secondary structure. In contrast, in the mutant protein, once α2 and α4 have lost their secondary structures, they are unable to recover. The most stable regions might be helix α2 in the WT protein and helix α3 in the mutant leptin; these regions maintain their helicity for the longest periods during the simulations. The interactions between Ile64-Leu90-S67 and Thr27-Ser67 are conserved in the WT leptin upon thermal denaturation and might contribute to the stabilization of helix α2. In contrast, these pairs are not observed in the mutant leptin after 3 ns of simulation at 500 K. Additionally, we noticed that the substitution of tryptophan for a glutamic acid at position 100 leads to the establishment of a network of electrostatic interactions, which stabilize helix α3. This network is mainly formed by R84, which is orientated towards E100 to form a salt bridge, and Q56 is attracted by the ions. This interaction represents a trade-off that increases the stability of α3 at the expense of the reduced stability of α2 in the mutant protein. Furthermore, the knot does not become unthreaded in either of the constructs. Thus, during the time course of the simulation, the N-terminus is incapable of unknotting through the inner space of the covalent loop. This loop contains the loop between α3 and α3´, as we mentioned, and this region moves away from the core of the protein, providing room for the N-terminus to unthread through the covalent loop. Nonetheless, the knot is maintained throughout the time course of the simulation at 500 K in both leptin constructs.

5. Concluding remarks

The conformational landscapes of WT and W100E leptin have been explored using molecular dynamics simulations at 300, 400 and 500 K. We concluded that the two constructs vary in their dynamical behavior, stability and unfolding pathway. We identified a network of interactions that differs between the leptin constructs and contributes to the dissimilarities in their structure and dynamical features. Additionally, these interactions might serve as safety locks to maintain helix α2 in the WT protein or helix α3 in W100E leptin upon thermal denaturation. In addition, we found that the region between residues 25 and 41 might be described as a putative intrinsically disordered region. The reasons for the presence of this unstructured region within leptin could be either structural or functional. Our findings might facilitate the therapeutic usage of leptin. However we still need to address this problem, by other biophysical approaches. We will investigate this in our future research.

Acknowledgments

This work received financial support by Medix; Project entitled “Generación de variantes de Leptina humana como alternativa terapéutica en el tratamiento de la obesidad y diabetes mellitus”. We also thank Grants SIP-IPN 20140317, 20140266, and 20140297. B. Chimal-Vega thanks scholarships from CONACyT (04042009) and Medix

Appendix A. Supplementary Information

Supplementary data associated with this article can be found in the online version at. 10.1016/j.jtbi.2015.08.014

References

Bax, A., et al., 2001. Solution structure of Ca2+-calmodulin reveals flexible hand-like properties of its domains. Nat. Struct. Biol. 8, 990–997.
Bence, K.K., Delibegovic, M., Xue, B., Gorgun, C.Z., Hotamisligil, G.S., Neel, B.G., Kahn, B.B., 2006. Neuronal PTP1B regulates body weight, adiposity and leptin action. Nat. Med. 12, 917–924.
Brenner, D., Makc, T.W., 2009. Mitochondrial cell death effectors. Curr. Opin. Cell Biol. 21, 871–877.

Berendsen, H.J.C., Postma, J.P.M., Van Gunsteren, W.F., Hermans, J., 1981. Interaction models for water in relation to protein hydration. In: Pullman, B. (Ed.), Intermolecular Forces. D. Reidel Publishing Company, Dordrecht, pp. 331–342.
Boute, N., Zilberfarb, V., Camoin, L., Bonnafous, S., Le Marchand-Brustel, Y., Issad, T., 2004. The formation of an intrachain disulfide bond in the leptin protein is necessary for efficient leptin secretion. Biochimie 86, 351–356.
Carpenter, B., Hemsworth, G.R., Wu, Z., Maamra, M., Strasburger, C.J., Ross, R.J., Artymiuk, P.J., 2012. Structure of the human obesity receptor leptin-binding domain reveals the mechanism of leptin antagonism by a monoclonal antibody. Structure 7, 487–497.
Chen, N.Y., et al., 1977. The biological functions of low-frequency phonons. Sci. Sin. 20, 447–457.
Chimal, V.B., Paniagua, C.N., Pérez, R.J.C., Carillo, V.J.P., Zamorano, C.A., Benítez, C.C. G., 2014. Antiobesity effects of human soluble leptin in mice nourished with a high-fat/high fructose diet. Am. J. Agric. Biol. Sci. 9, 430–438.
Chou, K.C., 1985. Low-frequency motions in protein molecules: beta-sheet and beta-barrel. Biophys. J. 48, 289–297.
Chou, K.C., 1989. Low-frequency resonance and cooperativity of hemoglobin. Trends Biochem. Sci. 14, 212–213.
Chou, K.C., 1998. Low-frequency collective motion in biomacromolecules and its biological functions. Biophys. Chem. 30, 3–48.
Daggett, V., 2006. Protein folding-simulation. Chem. Rev. 106, 1898–1916.
Day, R., Paschek, D., Garcia, A.E., 2010. Microsecond simulations of the folding/unfolding thermodynamics of the Trp-cage miniprotein. Proteins 78, 1889–1899.
Delarue, M., Sanejouand, Y.H., 2002. Simplified normal modeanalysis of conformational transitions in DNA-dependent polymerases: the elastic network model. J. Mol. Biol. 320, 1011–1024.
Dosztányi, Z., Csizmok, V., Tompa, P., Simon, I., 2005. IUPred: web server for the prediction of intrinsically unstructured regions of proteins based on estimated energy content. Bioinformatics 15, 3433–3434.
Du, Q.S., Chen, D., Xie, N.Z., 2014. Insight from studying a molecular interaction force supporting peptide backbones and its implication to protein loops and global folding. J. Biomol. Struct. Dyn. 33, 1957–1972.
Ducy, P., Amling, M., Takeda, S., Priemel, M., Schilling, A.F., Beil, F.T., Shen, J., Vinson, C., Rueger, J.M., Karsenty, G., 2000. Leptin inhibits bone formation through a hypothalamic relay: a central control of bone mass. Cell 21, 197–207.
Essmann, U., Perera, L., Berkowitz, M.L., Darden, T., Lee, H., Pedersen, L.G., 1995. A smooth particle mesh ewald potential. J. Chem. Phys. 103, 8577–8592.
Eswar, N., Marti-Renom, M.A., Webb, B., Madhusudhan, M.S., Eramian, D., Shen, M., Pieper, U., Sali, A., 2006. Comparative protein structure modelling with modeller. Current Protocols in Bioinformatics, pp. 5.6.1–5.6.30 (Supplement 15).
Fernandez Fuentes, N., Zhai, J., Fiser, A., 2006. ArchPRED: a template based loop structure prediction server. Nucleic Acids Res. 1 34 (Web Server issue: W), 173–176.
Flier, J.S., 1998. Clinical review 94: what's in a name? In search of leptin's physiologic role. J. Clin. Endocrinol. Metab. 83, 1407–1413.
Forsen, S., et al., 1981. The biological functions of low-frequency phonons: 2. Cooperative effects. Chem. Scr. 18, 126–132.
Gong, K., Li, L., Wang, J.F., Cheng, F., 2009. Binding mechanism of H5N1 influenza virus neuraminidase with ligands and its implication for drug design. Med. Chem. 5, 242–249.
Gordon, G., 2007. Designed electromagnetic pulsed therapy: clinical applications. J. Cell. Physiol. 212, 579–582.
Gordon, G., 2008. Extrinsic electromagnetic fields, low frequency (phonon) vibrations, and control of cell function: a non-linear resonance system. J. Biomed. Sci. Eng. 1, 152–156.
Haglund, E., Sułkowska, J.I., Zhao, H., Feng, G.S., Jennings, P.A., Onuchic, J.N., 2012. The unique cysteine knot regulates the pleotropic hormone leptin. PLoS One 7, 1–13.
Hess, B., Kutzner, C., Van der Spoel, D., Lindahl, E., 2008. GROMACS 4: algorithms for highly efficient, load-balanced, and scalable molecular simulation. J. Chem. Theory Comput. 4, 435–447.
Hess, B., Bekker, H., Berendsen, H.J.C., Fraaije, J.G.E.M., 1997. LINCS: a linear constraint solver for molecular simulations. J. Comput. Chem. 18, 1463–1472.
Heymsfield, S.B., Greenberg, A.S., Fujioka, K., Dixon, R.M., Kushner, R., Hunt, T., Lubina, J.A., Patane, J., Self, B., Hunt, P., McCamish, M., 1999. Recombinant leptin for weight loss in obese and lean adults: a randomized, controlled, dose-escalation trial. J. Am. Med. Assoc. 27, 1568–1575.
Holm, L., Sander, C., 1992. Evaluation of protein models by atomic solvation preference. J. Mol. Biol. 5, 93–105.
Hoover, W.G., 1985. Canonical dynamics: equilibriumphase-space distributions. Phys. Rev. A 31, 1695–1697.
Houseknecht, K.L., Baile, C.A., Matteri, R.L., Spurlock, M.E., 1998. The biology of leptin: a review. J. Anim. Sci. 76, 1405–1420.
Humphrey, W., Dalke, A., Schulten, K., 1996. VMD-visual molecular dynamics. J. Mol. Graphics 14, 33–38.
⟨http://www.pymol.org⟩ (PyMOL plugins are often called wizards, hence our choice of name).
⟨http://igs-server.cnrs.mrs.fr/elnemo/index.html⟩.
⟨https://salilab.org/modeller/⟩.
Jorgensen, W.L., Tirado-Rives, J., 1998. The OPLS potential functions for proteins, energy minimizations for crystals of cyclic peptides and crambin. J. Am. Chem. Soc. 110, 1657–1666.
Kabsch, W., Sander, C., 1983. Dictionary of protein secondary structure: pattern recognition of hydrogen-bonded and geometrical features. Biopolymers 22, 2577–2637.
Laskowski, R.A., MacArthur, M.W., Moss, D.S., Thornton, J.M., 1993. PROCHECK: a program to check the stereochemical quality ofprotein structures. J. Appl. Crystallogr. 26, 283–291.
Laskowski, R.A., Rullmannn, J.A., MacArthur, M.W., Kaptein, R., Thornton, J.M., 1996. AQUA and PROCHECK-NMR: programs for checking the quality of protein structures solved by NMR. J. Biomol. NMR 8, 477–486.
Li, L., Wei, D.Q., Wang, J.F., 2007. Computational studies of the binding mechanism of calmodulin with chrysin. Biochem. Biophys. Res. Commun. 358, 1102–1107.
Lo, K.M., Zhang, J., Sun, Y., Morelli, B., Lan, Y., Lauder, S., Brunkhorst, B., Webster, G., Hallakou-Bozec, S., Doaré, L., Gillies, S.D., 2005. Engineering a pharmacologically superior form of leptin for the treatment of obesity. Protein Eng. Des. Sel. 18, 1–10.
Lord, G.M., Matarese, G., Howard, J.K., Baker, R.J., Bloom, S.R., Lechler, R.I., 1998. Leptin modulates the T-cell immune response and reverses starvation-induced immunosuppression. Nature 27, 897–901.
Lüthy, R., Bowie, J.U., Eisenberg, D., 1992. Assessment of protein models with three-dimensional profiles. Nature 5, 83–85.
Madkan, A., et al., 2009. Steps to the clinic with ELF EMF. Nat. Sci. 1, 157–165. http://dx.doi.org/10.4236/ns.2009.13020, openly access at.
Maggiora, G.M., et al., 1989. Quasi-continuum models of twist-like and accordion-like low-frequency motions in DNA. Biophys. J. 56, 295–305.
Maggiora, G.M., et al., 1994. Solitary wave dynamics as a mechanism for explaining the internal motion during microtubule growth. Biopolymers 34, 143–153.
Mao, B., et al., 1988. Collective motion in DNA and its role in drug intercalation. Biopolymers 27, 1795–1815.
Martel, P., 1992. Biophysical aspects of neutron scattering from vibrational modes of proteins. Prog. Biophys. Mol. Biol. 57, 129–179.
Martí, A., Marcos, A., Martínez, J.A., 2001. Obesity and immune function relationships. Obes. Rev. 2, 131–140.
Masuzaki, H., Ogawa, Y., Sagawa, N., Hosoda, K., Matsumoto, T., Mise, H., Nishimura, H., Yoshimasa, Y., Tanaka, I., Mori, T., Nakao, K., 1997. Nonadipose tissue production of leptin: leptin as a novel placenta-derived hormone in humans. Nat. Med. 3, 1029–1033.
Melo, F., Devos, D., Depiereux, E., Feytmans, E., 1997. ANOLEA: a www server to assess protein structures. Am. Assoc. Artif. Intell. (www.aaai.org).
Molecular Operating Environmet versión2008.10.
Moschos, S., Chan, J.L., Mantzoros, C.S., 2002. Leptin and reproduction: a review. Fertil. Steril. 77, 433–444.
Nosé, S., Klein, M.L., 1983. Constant pressure molecular dynamics for molecular systems. Mol. Phys. 50, 1055–1076.
Nosé, S., 1984. A molecular dynamics method for simulations in the canonical ensemble. Mol. Phys. 52, 255–268.
Parrinello, M., Rahman, A., 1981. Polymorphic transitions in single crystals: a new molecular dynamics method. J. Appl. Phys. 52, 7182–7190.
Paz-Filho, G., Mastronardi, C., Delibasi, T., Wong, M.L., Licinio, J., 2010. Congenital leptin deficiency: diagnosis and effects of leptin replacement therapy. Arq. Bras. Endocrinol. Metab. 54, 690–697.
Pielak, R.M., Jason R., Schnell, J.R. Chou, J.J., 2009. Mechanism of drug inhibition and drug resistance of influenza A M2 channel. Proceedings of National Academy of Science, USA, vol. 106, pp. 7379–7384.
Prins, J.B., 2002. "Adipose tissue as an endocrine organ". Best Prac. Res. Clin. Endocrinol. Metab. 16, 639–651.
Ring, B.D., Scully, S., Davis, C.R., Baker, M.B., Cullen, M.J., Pelleymounter, M.A., Danilenko, D.M., 2000. Systemically and topically administered leptin both accelerate wound healing in diabetic ob/ob mice. Endocrinology 141, 446–449.
Schnell, J.R., Chou, J.J., 2008. Structure and mechanism of the M2 proton channel of influenza A virus. Nature 451, 591–595.
Seufert, J., Kieffer, T.J., Habener, J.F., 1999. Leptin inhibits insulin gene transcription and reverses hyperinsulinemia in leptin-deficient ob/ob mice. Proc. Natl. Acad. Sci. USA 19, 674–679.
Sierra-Honigmann, M.R., Nath, A.K., Murakami, C., García-Cardeña, G., Papapetropoulos, A., Sessa, W.C., Madge, L.A., Schechner, J.S., Schwabb, M.B., Polverini, P.J., Flores-Riveros, J.R., 1998. Biological action of leptin as an angiogenic factor. Science 11, 1683–1686.
Sinkala, Z., 2006. Soliton/exciton transport in proteins. J. Theor. Biol. 241, 919–927.
Suhre, K., Sanejouand, Y.H., 2004. ElNemo: a normal mode web server for protein movement analysis and the generation of templates for molecular replacement. Nucleic Acids Res. 1, 32.
Tama, F., Gadea, F.X., Marques, O., Sanejouand, Y.H., 2000. Building-block approach for determining low-frequency normal modes of macromolecules. Proteins 41, 1–7.
Tutone, M., Pantano, L., Lauria, A., Almerico, A.M., 2014. Molecular dynamics, dynamic site mapping, and highthroughput virtual screening on leptin and the Ob receptor as anti-obesity target. J. Mol. Model. 20, 2247.
Unger, R.H., Zhou, Y.T., Orci, L., 1999. Regulation of fatty acid homeostasis in cells: novel role of leptin. Proc. Natl. Acad. Sci. USA 2, 2327–2332.
Wang, J.F., Wei, D.Q., Li, L., Zheng, S.Y., 2007a. 3D structure modeling of cytochrome P450 2C19 and its implication for personalized drug design. Biochem. Biophys. Res. Commun. 355, 513–519 (Corrigendum: ibid).
Wang, J.F., Wei, D.Q., Lin, Y., Wang, Y.H., 2007b. Insights from modeling the 3D structure of NAD (P) H-dependent D-xylose reductase of Pichia stipitis and its binding interactions with NAD and NADP. Biochem. Biophys. Res. Commun. 359, 323–329.

Wang, J.F., Wei, D.Q., Chen, C., 2008a. Molecular modeling of two CYP2C19 SNPs and its implications for personalized drug design. Protein Pept. Lett. 15, 27–32.
Wang, J.F., Wei, D.Q., Du, H.L., 2008b. Molecular modeling studies on NADP-dependence of Candida tropicalis strain xylose reductase. The Open Bioinformatics Journal. 2, 72–79.
Wang, J.F., 2009. Insight into the molecular switch mechanism of human Rab5a from molecular dynamics simulations. Biochem. Biophys. Res. Commun. 390, 608–612.
Wang, J.F., Wei, D.Q., 2009. Insights from investigating the interactions of adamantane-based drugs with the M2 proton channel from the H1N1 swine virus. Biochem. Biophys. Res. Commun. 388, 413–417.
Wang, J.F., Gong, K., Wei, D.Q., 2009a. Molecular dynamics studies on the interactions of PTP1B with inhibitors: from the first phosphate-binding site to the second one. Protein Eng. Des. Sel. 22, 349–355.
Wang, J.F., Yan, J.Y., Wei, D.Q., 2009b. Binding of CYP2C9 with diverse drugs and its implications for metabolic mechanism. Med. Chem. 5, 263–270.
Wang, J.F., et al., 2009c. Insight into the molecular switch mechanism of human Rab5a from molecular dynamics simulations. Biochem. Biophys. Res. Commun. 390, 608–612.
Webb, B., Sali, A., 2014. Protein structure modeling with MODELLER. Methods Mol. Biol. 1137, 1–15.
Zhang, F., Basinski, M.B., Beals, J.M., Briggs, S.L., Churgay, L.M., Clawson, D.K., DiMarchi, R.D., Furman, T.C., Hale, J.E., Hsiung, H.M., Schoner, B.E., Smith, D.P., Zhang, X.Y., Wery, J.P., Schevitz, R.W., 1997. Crystal structure of the obese protein leptin-E100. Nature 8, 206–209.
Zhang, Y., 2008. I-TASSER server for protein 3D structure prediction. BMC Bioinform. 23 9:40.
Zhang, Y., Proenca, R., Maffei, M., Barone, M., Leopold, L., Friedman, J.M., 1995. Positional cloning of the mouse obese gene and its human homologue. Nature 372, 425–432.
Zhou, G.P., 1989. Biological functions of soliton and extra electron motion in DNA structure. Phys. Scr. 40, 698–701.